

Cite this: *Nanoscale*, 2018, 10, 3281

## *In situ* tribochemical sulfurization of molybdenum oxide nanotubes

 Manel Rodríguez Ripoll,<sup>a</sup> Agnieszka Tomala,<sup>a,b</sup> Christoph Gabler,<sup>a</sup>  
 Goran Dražić,<sup>c,d</sup> Luka Pirker<sup>d</sup> and Maja Remškar<sup>d</sup>

MoS<sub>2</sub> nanoparticles are typically obtained by high temperature sulfurization of organic and inorganic precursors under a S rich atmosphere and have excellent friction reduction properties. We present a novel approach for making the sulfurization unnecessary for MoO<sub>3</sub> nanotubes during the synthesis process for friction and wear reduction applications while simultaneously achieving a superb tribological performance. To this end, we report the first *in situ* sulfurization of MoO<sub>3</sub> nanotubes during sliding contact in the presence of sulfur-containing lubricant additives. The sulfurization leads to the tribo-chemical formation of a MoS<sub>2</sub>-rich low-friction tribofilm as verified using Raman spectroscopy and can be achieved both during sliding contact and under extreme pressure conditions. Under sliding contact conditions, MoO<sub>3</sub> nanotubes in synergy with sulfurized olefin polysulfide and pre-formed zinc dialkyl dithiophosphate tribofilms achieve an excellent friction performance. Under these conditions, the tribochemical sulfurization of MoO<sub>3</sub> nanotubes leads to a similar coefficient of friction to the one obtained using a model nanolubricant containing MoS<sub>2</sub> nanotubes. Under extreme pressure conditions, the *in situ* sulfurization of MoO<sub>3</sub> nanotubes using sulfurized olefin polysulfide results in a superb load carrying capacity capable of outperforming MoS<sub>2</sub> nanotubes. The reason is that while MoO<sub>3</sub> nanotubes are able to continuously sulfurize during sliding contact conditions, MoS<sub>2</sub> nanotubes progressively degrade by oxidation thus losing lubricity.

Received 7th August 2017,  
Accepted 8th January 2018

DOI: 10.1039/c7nr05830f

rsc.li/nanoscale

## 1. Introduction

Friction and wear reduction in machine elements and industrial components is a major target that aims to solve two major problems of our society simultaneously. The economic costs caused by frictional losses and machinery downtime due to replacement of worn components are by themselves a major concern. In 2005, the founding father of tribology Peter Jost summarized studies performed in different countries that indicated potential savings of up to 1.4% of the gross national product by introducing better tribological practices.<sup>1</sup> Besides the more obvious economic costs associated with friction and wear losses, environmental regulations have played a key role in driving research in tribology during the past 20 years. In automotive components, frictional losses are intimately related to fuel consumption and emission of greenhouse gases.<sup>2</sup> Hence, the often ambitious targets set by legislators for reducing our CO<sub>2</sub> footprint require the development of novel and greener lubrication concepts for reducing friction and

wear.<sup>3</sup> Within this context, layered materials have emerged as one of the potential candidates for achieving these goals.<sup>4</sup>

Transition metal dichalcogenides were some of the first layered compounds that were found to be suitable for friction reduction. Thanks to their 2D hexagonal arrangement, some transition metal dichalcogenides (TMDs), such as MoS<sub>2</sub> have a 2D structure, characterized by a transition metal atom sandwiched between two chalcogen atoms forming a layer of the form S–Mo–S.<sup>5</sup> Adjacent layers interact weakly and are held together by van der Waals interactions. As a consequence of this 2D structure and the weak interaction between adjacent planes, TMDs have a low sliding energy surface corrugation which results in easy shear between lamellas and consequently, in an overall low friction.<sup>4</sup> *Ab initio* calculations have recently explored the frictional properties of TMDs as a function of chemical composition and bilayer orientation for showing the relationship between incommensurate crystals and superlubricity.<sup>6</sup>

Initially, TMDs were applied to sliding components as burnished or sputtered coatings and their application was limited to the context of space lubrication due to their poor performance in humid air.<sup>7</sup> However, after the pioneering synthesis of TMDs as inorganic fullerene nanoparticles,<sup>8,9</sup> their application as a potential lubricant additive was soon envi-

<sup>a</sup>AC2T research GmbH, Wiener Neustadt, Austria. E-mail: ripoll@ac2t.at<sup>b</sup>Institute for Sustainable Technologies, Radom, Poland<sup>c</sup>National Institute of Chemistry, Ljubljana, Slovenia<sup>d</sup>Institute Jožef Stefan, Ljubljana, Slovenia

saged.<sup>10</sup> Shortly later, other morphologies<sup>11</sup> and closed-cage nanostructures<sup>12,13</sup> could be successfully synthesized. Since then, the number of studies showing the superb performance of nanolubricants containing TMD nanoparticles for lubricating metals and coatings under several contact conditions has been very vast.<sup>14–18</sup>

The synthesis of TMD nanoparticles can be accomplished using different techniques but the majority of them rely on the sulfurization of transition metal inorganic compounds, such as  $\text{MO}_3$ ,  $\text{MCl}_5$ ,  $\text{MF}_6$ ,  $\text{Mo}_6\text{S}_x\text{I}_y$ ,  $\text{WO}_x$ - $\text{W}_{18}\text{O}_{49}$  or transition metal-organic precursors, such as  $\text{M}(\text{S}-t\text{-Bu})_4$ ,  $\text{M}(\text{CO})_6$  at high temperature mostly in the presence of  $\text{H}_2\text{S}$  or a similar sulfur compound<sup>18–24</sup> according to the following chemical reaction:<sup>25</sup>



More recently, this procedure has been extended to the synthesis of complex hybrid composite nanoparticles containing transition metal dichalcogenides and carbon, either as nanotubes<sup>26</sup> or graphene.<sup>27</sup> An analogous high temperature approach is used for the synthesis of  $\text{WS}_2$  and  $\text{WSe}_2$  monolayers for electronics using a  $\text{WO}_3$  precursor.<sup>28–30</sup> Consequently, an *in situ* sulfurization of TM-based precursor nanoparticles during operation would provide an economical option for skipping the sulfurization step thus improving the overall efficiency of the process by reducing costs and saving energy. One of the main prerequisites for the proliferation and establishment of TMD nanoparticles as friction modifiers in commercial fully formulated products lies in their ready availability in large quantities.

The sulfurization of transition metal precursors requires the use of high temperature and/or pressure. Since both the conditions are typically found at the contact interface between sliding bodies due to the high pressures and temperatures locally occurring at interacting asperities,<sup>31</sup> it seems plausible to postulate that the energy required for the sulfurization product could be achieved by these means. This approach implicitly assumes the simultaneous presence of transition metal oxide nanoparticles and sulfur species in the lubricant formulation. The latter condition is nowadays already fulfilled by most of the common commercially available lubricants, since they contain anti-wear additives such as zinc dialkyl dithiophosphate (ZDDP) or extreme pressure additives, such as sulfurized olefins.<sup>32</sup>

The aim of this work is to promote the *in situ* sulfurization of molybdenum oxide nanotubes using conventional sulfur-containing lubricant additives such as a ZDDP anti-wear additive and a sulfurized-olefin extreme pressure additive. The approach is verified giving special emphasis to the role of the additive chemistry and contact conditions. The results show an exceptional performance in terms of friction and wear when compared to the results obtained using  $\text{MoS}_2$  nanotubes alone, thus proving that, for friction reduction applications, the sulfurization of transition metal oxide nanoparticles during the synthesis process might be superfluous by utilizing the present approach.

## 2. Experimental

### 2.1 $\text{MoO}_3$ nanotubes

The  $\text{MoO}_3$  nanotubes were synthesized in two-steps.<sup>33</sup> Firstly, the precursor  $\text{Mo}_6\text{S}_2\text{I}_8$  nanowires were prepared from the stoichiometric amounts of molybdenum (Aldrich 99.9%), sulfur (Aldrich 99%) and iodine (Sigma-Aldrich reagent-plus grade) in evacuated and sealed silica ampoules at 736 °C using a temperature gradient of 5.5 K  $\text{cm}^{-1}$ . The obtained nanowires had a length of 5  $\mu\text{m}$  and a diameter in the range of 100–200 nm. These nanowires were subsequently oxidized for 25 hours in ambient air at 573 K. The  $\text{MoO}_3$  nanotubes were composed of polycrystalline  $\text{MoO}_{3-x}$  nanowires and nanotubes arranged in hedgehog-like self-assemblies (Fig. 1a). The facetting tendency of the nanotubes (Fig. 1b and d) was explained with the faster growth along the  $(0k0)$  planes in comparison with the growth in the perpendicular  $[0k0]$  direction. A high-resolution TEM image (Fig. 1c-inset) shows a periodicity of 3.7 Å along the nanotube's axis, which matches the  $(001)$  interlayer distance of  $\alpha\text{-MoO}_3$  (3.697 Å), and 6.8 Å periodicity in a perpendicular direction, which is close to the  $(020)$  interlayer distance of  $\alpha\text{-MoO}_3$  (6.93 Å). The calculated BET surface is  $14.3 \pm 0.3 \text{ m}^2 \text{ g}^{-1}$  and the degree of oxygen deficiency ( $x$ ) was estimated to be 0.002.<sup>33</sup> All peaks in the X-ray diffraction spectrum (Fig. 1d) of  $\text{MoO}_3$  powder are in agreement with the orthorhombic  $\alpha\text{-MoO}_3$  phase (JCPDS No. 05-0508). Some of the peaks are labelled for the qualitative comparison with bulk  $\text{MoO}_3$ . Relatively weak  $(0k0)$  diffraction peaks with regard to the intensities from the database are explained with the fact that the walls of the nanotubes are composed of thin flakes with thickness along the  $[0k0]$  direction.

### 2.2 Lubricant mixtures

The lubricant mixture for the sliding tests contained poly-alpha olefin 4 (PAO) base oil with 5 wt%  $\text{MoO}_3$  nanotubes and either a 2 wt% zinc dialkyl dithiophosphate (ZDDP) anti-wear additive, with a primary alkyl structure and 99% purity or 2 wt% sulfurized olefin polysulphide (40% of sulfur content) extreme-pressure (EP). The PAO base oil had a viscosity of 4  $\text{mm}^2 \text{ s}^{-1}$  at 100 °C. For the Brugger tests, the poly-alpha olefin 4 (PAO) base oil was mixed with 2 wt% sulfurized olefin polysulphide (40% of sulfur content) extreme-pressure. Both lubricant additives were obtained from Lukoil Lubricants Europe (Austria). The mixtures were homogenized by applying an ultrasonic processor VC 505 (Sonics & Materials, Inc, USA). The selected parameters at the probe tip were 20% amplitude during 8 min, while the pulse was on and off for 2 seconds, respectively. For comparison, a mixture was used containing poly-alpha olefin 4 (PAO) base oil with 5 wt%  $\text{MoS}_2$  nanotubes. The details regarding this mixture can be found elsewhere.<sup>34</sup>

### 2.3 Tribological tests

The tribological tests were performed on a SRV® tribometer (Optimol Instruments Prüftechnik GmbH, Germany) under reciprocating sliding conditions using a point of contact at 40 °C. The selected material for the testing discs was AISI



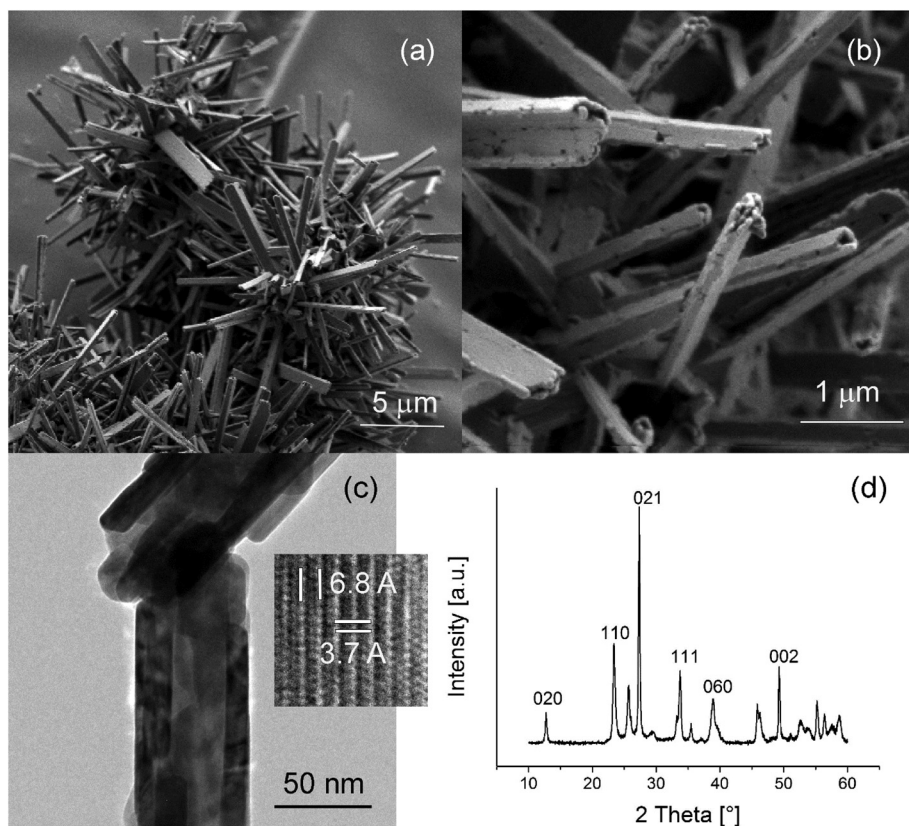


**Fig. 1** MoO<sub>3</sub> nanotubes and nanowires: (a) SEM image of hedgehog-like self-assemblies of MoO<sub>3</sub> nanowires and nanotubes; (b) SEM image of faceted MoO<sub>3</sub> nanotubes with a high degree of porosity; (c) TEM image revealing the polycrystalline structure of MoO<sub>3</sub> nanotubes growing along the [001] direction with a high resolution image of the nanotube's wall; (d) XRD pattern with some peaks assigned according to the  $\alpha$ -MoO<sub>3</sub> (JCPDS No. 05-0508).

52100 bearing steel with a microstructure formed by fine martensitic iron and disperse micrometer size carbides, which resulted in a hardness of 850 HV10 and a roughness of  $R_a$  0.05  $\mu\text{m}$ . As counterbody, also AISI 52100 bearing steel balls with a diameter of 10 mm were used with the same hardness and roughness. All samples were carefully cleaned before the tests in an ultrasonic bath for 10 minutes with toluene and subsequently, 10 additional minutes with petroleum ether. The normal load was kept constant at a 25 N throughout the test, which resulted in an initial average Hertzian contact pressure of 0.9 GPa. The oscillation amplitude was set to 1.5 mm and the test was run at 25 Hz for one hour with the aim of allowing sufficient time for tribochemical reactions to take place and to reach steady-state friction values.

Selected samples were tested under extreme pressure conditions using the Brugger test according to DIN 51347-1 and 2. The Brugger test is a standard procedure used to determine the performance of lubricants. The Brugger test is particularly suitable for promoting the reaction of active additives, particularly extreme pressure, but is less sensitive to adsorptive agents. The Brugger test is performed at room temperature in a Brugger apparatus where a rotating test cylinder with a circumferential velocity of 1.25  $\text{m s}^{-1}$  is pressed with 400 N (mean contact pressure of 1.9 GPa) against a fixed cylinder

placed with the axis perpendicular to the test cylinder. After the test, the Brugger-value defined as the ratio between the normal load and the area of the wear scar is measured and gives a value for the load carrying capacity of the investigated lubricant. The test specimens used for the Brugger tests were also made of AISI 52100 bearing steel and had a hardness of 60 HRC and roughness  $R_a < 0.8$  for the friction ring (25 mm diameter) and a hardness of 65 HRC and roughness  $R_a < 0.2 \mu\text{m}$  for the test cylinder (8 mm diameter). A summary of the test parameters is given in Table 1.

**Table 1** Summary of the used parameters for every test setup

	SRV® test	Brugger test
Contact	Point	Elliptic
Loading condition	Reciprocating sliding	Unidirectional sliding
Stroke	1.5 mm	—
Speed	0.04 $\text{m s}^{-1}$	1.25 $\text{m s}^{-1}$
Normal load	25 N	400 N
Mean contact pressure	0.9 GPa	1.9 GPa
Maximum contact pressure	1.4 GPa	2.9 GPa
Temperature	40 °C	23 °C
Test duration	1 h	30 s





## 2.4 Analyses of the *in situ* sulfurized tribofilms

The morphology of the tribofilms formed during the reciprocating sliding tests was characterized using a JEOL JSM 6500F scanning electron microscope operating with an acceleration voltage of 20 kV. Relevant features of the tribofilms were investigated using electron dispersive X-ray diffraction (EDX) in order to reveal their elemental composition.

The morphology of the tribofilm present after using a mixture of MoO<sub>3</sub> nanotubes with an extreme pressure additive on a well-established ZDDP tribofilm was investigated in a high resolution scanning transmission electron microscope mode (STEM) using a Cs-corrected JEOL ARM 200 CF STEM operating at 200 kV. The goal was to obtain a high resolution image of the tribofilm.

Raman spectroscopy was performed using a WITec Alpha 300 RS scanning confocal Raman microscope in a backscattered geometry using frequency doubled Nd:YAG 532 nm laser that was focused through a 100× objective with N.A. = 0.9. The power of the laser beam at the sample was 7 mW.

X-ray photoelectron spectroscopy (XPS) analyses were performed using a Thermo Fisher Scientific Theta Probe equipped with a monochromatic Al K $\alpha$  X-ray source ( $h\nu$  = 1486.6 eV) and an Ar<sup>+</sup> ion gun. During the measurements, the base pressure inside the XPS chamber was kept constant at values in the range of 10<sup>-7</sup> Pa. The investigated samples were ultrasonically cleaned in toluene followed by petroleum ether (both HPLC grade) before the tests and subsequently sputtered in the XPS chamber using soft Ar<sup>+</sup> for 20 seconds, with 3 kV and 1  $\mu$ A sputter current in order to remove the remaining contaminants. The high resolution spectra were taken at a pass energy of 50 eV and the resulting binding energies were referenced to adventitious carbon at a binding energy of 284.6 eV.

## 3. Results and discussion

### 3.1 Friction performance of the nanolubricant mixtures

The friction performance as a function of time of the lubricant mixture containing MoO<sub>3</sub> nanotubes is shown in Fig. 2. The results show that the mixture containing MoO<sub>3</sub> nanotubes and the ZDDP additive leads to an initial brief running-in period with a coefficient of the friction value close to 0.05 for subsequently stabilizing at a value of 0.08. As guidance, the friction level achieved by the reference PAO oil without the addition of any nanoparticle and/or additive was 0.15, so that the addition of the mixture containing MoO<sub>3</sub> nanotubes with the ZDDP additive results in a friction reduction of about 40%. This significantly lower friction value highlights the synergy between the MoO<sub>3</sub> nanotubes and the sulfur containing ZDDP. However, despite the dramatic reduction in friction, this value is still 30% higher than the coefficient of friction of *ca.* 0.06 achieved by the mixture containing only MoS<sub>2</sub> nanotubes.

The morphology of the wear track tested with MoO<sub>3</sub> and ZDDP reveals very little signs of wear and the original grinding marks present due to sample preparation are still visible inside the wear track (Fig. 3a). Only at higher magnifications,

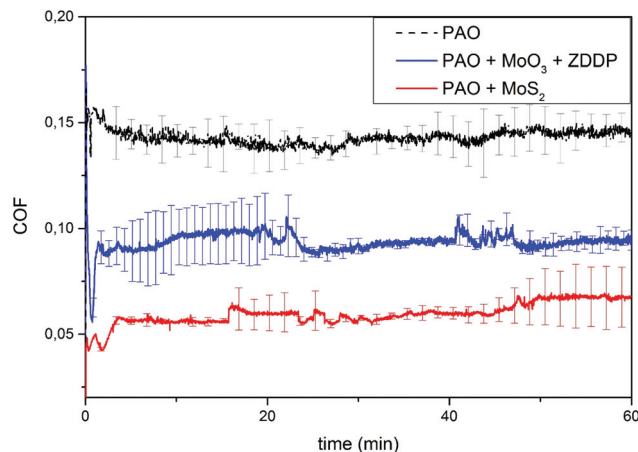


**Fig. 2** Coefficient of friction as a function of time for the lubricant mixtures containing 5 wt% MoO<sub>3</sub> nanotubes with the 2 wt% ZDDP anti-wear additive and 5 wt% MoS<sub>2</sub> nanotubes. The friction value obtained for pure PAO base oil is shown as a reference value.

minor signs of plastic deformation are visible, particularly at the edges of the grinding marks (Fig. 3a-inset). Subtle abrasive marks are also seen running parallel to the sliding direction, indicating the occurrence of mild two-body abrasion. The elements found in this area of the wear track correspond to Mo, Fe and O, indicating the possible presence of MoO<sub>3</sub> nanotube remains over the Fe substrate. The outer upper and lower edges of the wear track display darker regions with complete lack of surface degradation. The presence of Zn and S suggests the formation of a ZDDP tribofilm. These observations highlight the excellent performance of this lubricant mixture not only in terms of friction, but also in wear and evidenced that the superb anti-wear properties of ZDDP are preserved, when used in conjunction with MoO<sub>3</sub> nanotubes.

ZDDP is known to provide wear protection to steel substrates by forming a soft tribofilm containing Zn, S and P that is continuously formed and removed, acting as a sacrificial layer. However, this wear protection mechanism comes at a cost of a high friction.<sup>35</sup> Therefore, the presence of a ZDDP tribofilm alone cannot justify the friction results observed in the sliding experiments. To this end, the Raman spectroscopy measurement of the wear track was performed with the aim of identifying the presence of lubricating species. An optical image of the position inside the wear track, where the Raman spectra were measured, Raman mapping and spectra are shown in Fig. 3b–d. Two peaks at 377 cm<sup>-1</sup> and 403 cm<sup>-1</sup> characteristic for MoS<sub>2</sub><sup>36</sup> dominated the Raman spectrum. Also the broad peaks at 190 cm<sup>-1</sup>, 447 cm<sup>-1</sup> and 570 cm<sup>-1</sup> can be assigned to MoS<sub>2</sub>.<sup>37</sup> In order to estimate the surface distribution of the *in situ* formed MoS<sub>2</sub>, a Raman Mapping Image was acquired (Fig. 3c). The bright (yellow) area indicates a strong MoS<sub>2</sub> Raman signal (Fig. 3d-spectrum A), whereas the red/black area represents the absence of the MoS<sub>2</sub> Raman signal (spectrum B). The elongated distribution of MoS<sub>2</sub> overlaps with the darker areas observed on the optical image and



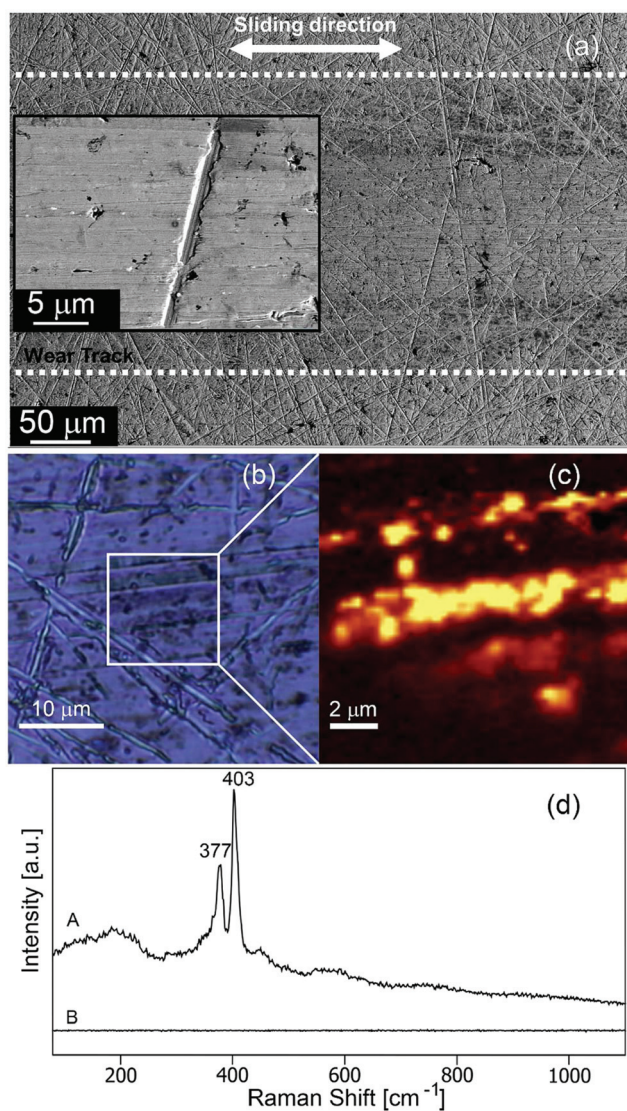


**Fig. 3** Analyses of the sample lubricated with the mixture containing 5 wt% MoO<sub>3</sub> nanotubes and the 2 wt% ZDDP antiwear additive: (a) wear scar showing a dark tribofilm at the upper and lower edges. At a higher resolution, a detailed of the central part of the wear track; (b) optical image of the selected area for Raman spectroscopy; (c) Raman Mapping Image formed from the Raman signal in the range of 350 to 430 cm<sup>-1</sup>; (d) Raman spectrum (A) measured at the bright (yellow) area, and Raman spectrum (B) measured at the black area.

is parallel to the sliding direction. Thus, the Raman data indicate that the *in situ* formation of MoS<sub>2</sub> from MoO<sub>3</sub> nanotubes during the sliding contact process in the presence of the ZDDP antiwear additive is feasible and explains the observed friction reduction. The *in situ* formation MoS<sub>2</sub> can also be achieved using organo molybdenum compounds such as MoDTC in combination with ZDDP.<sup>35</sup> However, these compounds pose environmental concerns.

For comparison, the sample tested using the lubricant mixture of PAO with MoS<sub>2</sub> nanotubes was also investigated using Raman spectroscopy measurements (Fig. 4). First, the

background signal of the substrate outside the wear track was measured. The wear track reveals the characteristic presence of a dark grey tribofilm (Fig. 4a), as a consequence of the tribofilm formed by exfoliation of MoS<sub>2</sub> lamellas during sliding contacts.<sup>14</sup> The presence of Mo on the tribofilm is evidenced by energy dispersive X-ray spectroscopy EDX (Fig. 4b). Raman spectroscopy measurements outside the wear track show that most of the sample surface has no Raman signal. However, in some individual spots, peaks are observed at 384 and 410 cm<sup>-1</sup>, which are characteristic for MoS<sub>2</sub> nanotubes.<sup>38</sup> This indicates that parts of the sample are in spite of cleaning still covered with traces of MoS<sub>2</sub>. Raman measurements performed on the wear track (Fig. 4c) show a weak MoS<sub>2</sub> signal with peaks at 381 and 407 cm<sup>-1</sup>. The two peaks are characteristic for the bulk MoS<sub>2</sub> crystal.<sup>36</sup>

### 3.2. *In situ* formation of MoS<sub>2</sub> on pre-formed ZDDP tribofilms

In the previous section, we proved the feasibility of sulfurizing *in situ* MoO<sub>3</sub> nanotubes during sliding contact under the presence of the ZDDP anti-wear additive. The morphology and chemical composition of the wear tracks clearly resemble the characteristics observed on samples tested with a lubricant mixture containing only MoS<sub>2</sub> nanotubes. However, the friction performance achieved by the *in situ* sulfurization is still far from the one reached by MoS<sub>2</sub> nanotubes. With the aim of understanding this difference thus providing further insights into the *in situ* reaction mechanism, we modify the lubricant mixtures in order to explore whether a similar performance can be obtained using our *in situ* sulfurization approach. In previous studies, we and other authors have remarked the synergy between TMD nanoparticles and ZDDP tribofilms.<sup>17,34,39,40</sup> ZDDP tribofilms have a typical thickness of about 100 nm, are amorphous and have a low hardness. Once a well-established ZDDP is formed, it facilitates trapping of nanoparticles and exfoliation of TMD lamellas on top of it, providing the ZDDP tribofilm with a top layer of about 10 nm thickness of exfoliated nanoparticles with excellent friction reduction properties.<sup>17</sup> ZDDP tribofilms are readily available in many lubricated components in automotive industry due to the widely spread use of this additive for anti-wear protection.

Based on these facts, a test series was performed, where the samples were initially rubbed for two hours with a mixture of PAO base oil and the ZDDP additive until a well-established ZDDP tribofilm was formed. After this initial 2 hours, the remaining lubricant was carefully removed and a lubricant mixture containing MoO<sub>3</sub> nanotubes with the sulfurized olefin EP additive was added and the test proceeds for two additional hours. The pursued idea was to use the ZDDP tribofilm as a trap for MoO<sub>3</sub> nanoparticles while they undergo *in situ* sulfurization by using the highly reactive EP additive as a sulfur source. This additive was proved effective for forming *in situ* low friction tribofilms on WC containing surfaces.<sup>41,42</sup>

The results of the experiment are shown in Fig. 5. During the initial two hours, the coefficient of friction lies at a high value of 0.17. As expected, ZDDP tribofilms are well-known for





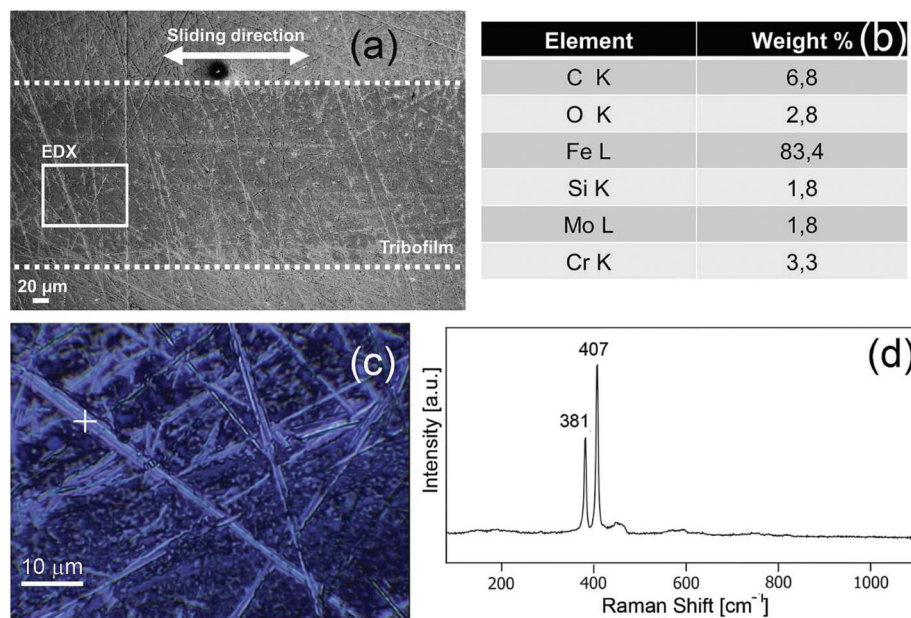


Fig. 4 Analyses of the sample lubricated with the mixture containing 5 wt% MoS<sub>2</sub> nanotubes: (a) wear scar showing a dark tribofilm using 2 kV acceleration voltage; (b) elemental composition of the tribofilm obtained by EDX; (c) position of the wear track (cross) where the Raman spectroscopy measurements were performed; (d) Raman spectrum with the characteristic peaks for MoS<sub>2</sub> at 381 and 407 cm<sup>-1</sup>.

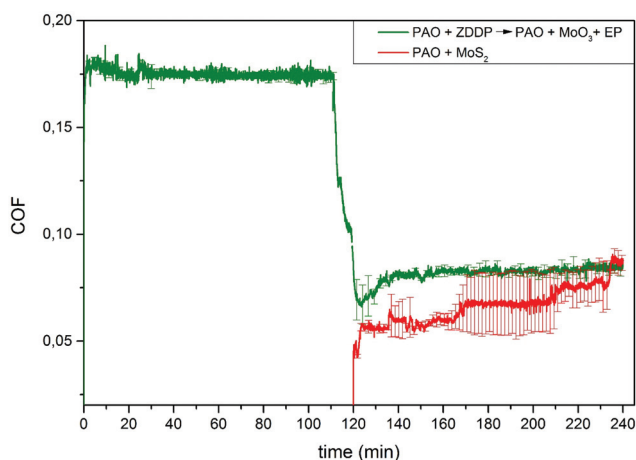


Fig. 5 Coefficient of friction as a function of time for the lubricant mixtures containing 5 wt% MoO<sub>3</sub> in combination with the 2 wt% EP additive when running on a ZDDP tribofilm pre-formed during the initial 2 hours of rubbing. The friction value obtained with a lubricant containing 5 wt% MoS<sub>2</sub> nanotubes is shown as a reference value.

its superb wear protection but do not improve the frictional properties of surfaces.<sup>17,35</sup> After two hours rubbing, as soon as the mixture containing ZDDP was replaced by a mixture containing MoO<sub>3</sub> nanotubes and the EP additive, an immediate dramatic reduction in friction was observed. The coefficient of friction decreases down to values of 0.06 for subsequently stabilizing at 0.08. These results provide an improvement when compared to the performance of the lubricant mixture containing MoO<sub>3</sub> and ZDDP. In analogy to reaction (1), it is plausible

to assume that the sulfurized olefin R-S-S-R reacts with the MoO<sub>3</sub> to produce MoS<sub>2</sub> according to the following reaction:



In case of a lubricant mixture containing MoS<sub>2</sub> nanotubes, the coefficient of friction is initially lower as reported previously, but rises to a final value of 0.08 after 120 minutes, a similar value as the one achieved by MoO<sub>3</sub> nanotubes with the EP additive. The reason for the friction increase is likely to occur due to the oxidation of MoS<sub>2</sub> to MoO<sub>3</sub>. It has been reported in the literature that under severe contact conditions and/or at elevated temperatures, WS<sub>2</sub> oxidizes in the tribocontact leading to the formation of WO<sub>3</sub>, which hampers the superb lubrication performance of WS<sub>2</sub>.<sup>14,43,44</sup>

The surface morphology after the test reveals the lack of the wear track. Absolutely no difference in the surface topography can be observed between the inner wear track and the rest of the surface. The reason is attributed to the excellent anti-wear performance of ZDDP (Fig. 6a). At the turning points of the wear track, the presence of darker patch areas indicates tribofilm formation (Fig. 6b). The elemental composition of the darker areas of the tribofilm reveals the presence of elements typically present in ZDDP tribofilms, such as Zn and S. In the rest of the wear track, the only elements detected after the experiment were Mo and O.

A lamella parallel to the sliding direction was cut using a focused ion beam (FIB). The selected region of interest was at the turning point of the wear track, where the dark color indicated the presence of a tribofilm formed (Fig. 6b). During the preparation, the region of interest was covered with a protective Pt/Pd film to avoid damaging the tribofilm. Afterwards,



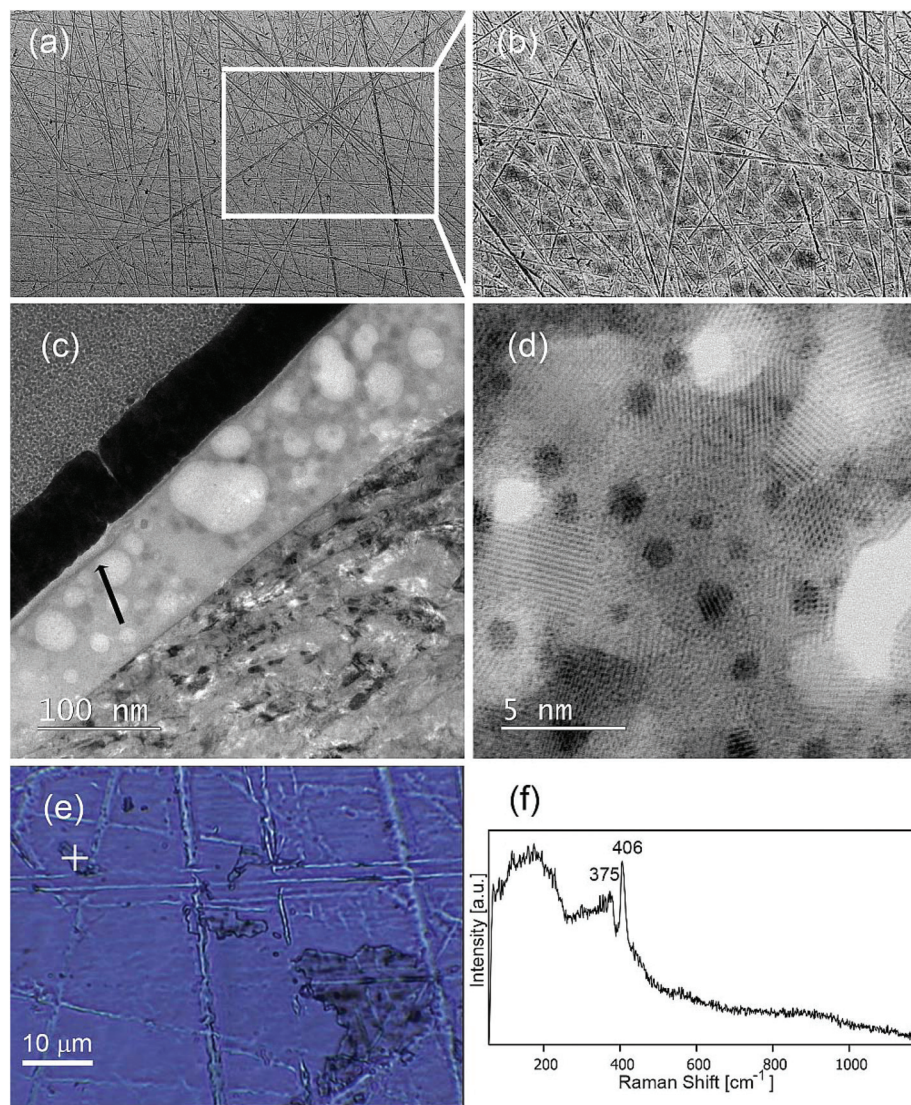


**Fig. 6** Analyses of the sample lubricated with the mixture containing 5 wt%  $\text{MoO}_3$  nanotubes and 2 wt% EP additive on a pre-formed ZDDP tribofilm: (a) wear track with no signs of wear; (b) darker patch-like tribofilm at the turning points; (c) cross-section of the turning point of the wear track with a tribofilm showing a bottom ZDDP tribofilm and an upper 10 nm light grey tribofilm; (d) crystallites of hexagonal ZnO inside the bottom tribofilm; (e) position of the wear track (cross) where the Raman spectroscopy measurements were performed; (f) Raman spectrum with the characteristic peaks for  $\text{MoS}_2$  at 375 and 406  $\text{cm}^{-1}$ .

the lamella was analysed using high resolution transmission electron microscopy (TEM). The TEM images show the presence of a tribofilm on top of the bearing steel surface with a thickness of about  $100 \pm 10$  nm (Fig. 6c). A closer inspection into the tribofilm morphology shows the presence of an initial bottom layer with a thickness covering most of the 100 nm and a very thin layer of less than 10 nm on top of it (marked with arrow). EDX analyses of the bottom tribofilm layer indicate the presence of Zn and S. The high resolution images verify the presence of hexagonal ZnO crystals characteristic of ZDDP tribofilms (Fig. 6d). The top layer part of tribofilm resembles the morphology of exfoliated  $\text{MoS}_2$  sheets, as observed when using  $\text{MoS}_2$  nanotubes,<sup>17</sup> but was too thin to be accurately analyzed using TEM-EDX. Therefore, the chem-

istry of this thin layer was analyzed from the top using Raman spectroscopy. Again, the background signal outside the wear track was analyzed and did not show any visible peaks. Inside the wear track, it was possible to find areas where peaks that are typical for  $\text{MoS}_2$  could be detected. A Raman spectrum obtained inside the wear track is shown in Fig. 6f, with two peaks at 375 and 406  $\text{cm}^{-1}$ . These peaks are a relatively good match for peaks that are characteristic for  $\text{MoS}_2$ . The spectrum was obtained on one of the patches as shown in Fig. 6e. The broad peak in the 100–250  $\text{cm}^{-1}$  region is in the literature attributed to the stress-induced disorder in the  $\text{MoS}_2$  crystal structure.<sup>45</sup> This peak is present only in the spectra, where  $\text{MoS}_2$  formed *in situ* (Fig. 3d and 6f), while it is absent in the spectrum corresponding  $\text{MoS}_2$  nanotubes in PAO oil (Fig. 4d).





One can expect that the crystal structure of  $\text{MoS}_2$ , which forms *in situ* from  $\text{MoO}_3$  and sulfur containing additives during a dynamic tribological process, is disordered not only due to stress, but also due to the formation process which is far from the equilibrium necessary for forming defect free compounds.

### 3.3 *In situ* tribochemical sulfurization under extreme pressure conditions

Until now, we discussed the feasibility of sulfurizing *in situ*  $\text{MoO}_3$  nanotubes in the context of mild sliding conditions. These conditions are characteristic of many components, such as those found in automotive components. However, many relevant machine elements operate under demanding conditions where higher sliding speeds and contact pressures are present. It has been recently showed that TMD nanoparticles may be an excellent option for reducing friction and wear under such conditions.<sup>34,43,46</sup> The reason lies in the ability of TMD nanoparticles for forming complex tribofilms formed by exfoliated TMD lamellas accompanied with the presence of iron sulfides that form at the contact interface with superb tribological properties.<sup>32,46</sup> These kinds of tribofilms can also be formed by TMD nanotubes under the presence of lubricant additives in model oils.<sup>34</sup>

Hence, we aim to show the feasibility of applying the *in situ* sulfurization of  $\text{MoO}_3$  nanotubes in sliding contacts using severe contact conditions. Our investigations rely on the Brugger test, which is an experiment widely used for characterizing the performance of lubricant additives under extreme pressure conditions. The lubricant mixtures selected were  $\text{MoO}_3$  nanotubes with a sulfurized olefin EP additive. The reason for this selection is that sulfurized olefins are the standard additive for extreme pressure conditions due to their high reactivity with Fe substrates to form protecting  $\text{FeS}$  and  $\text{FeSO}_4$  tribofilms. Since they are highly reactive, it is plausible to assume that they may be able to sulfurize  $\text{MoO}_3$  nanotubes during the experiment. For comparison, base PAO oil and a mixture containing  $\text{MoS}_2$  nanotubes alone were selected as a reference.

The results obtained are shown in terms of load carrying capacity (LCC) according to Brugger, *i.e.* the ratio between the normal load and the wear scar diameter. A higher LCC indicates a better extreme pressure performance of the lubricant. The results show that the lubricant mixture containing  $\text{MoO}_3$  and the EP additive has a superb LCC, significantly better than the mixture containing only the EP additive (Fig. 7a). This result hints a different and more efficient lubrication mechanism. In case of sulfur-containing EP additives, the lubrication mechanism under EP conditions relies on the formation of a sacrificial soft  $\text{FeS}$  tribofilm, which prevents metal to metal contact. Under the presence of  $\text{MoO}_3$ , since the sulfur content of both mixtures is identical, the mechanism needs to be different. The answer may be revealed by X-ray photoelectron spectroscopy measurements, which verify the *in situ* formation of  $\text{MoS}_2$  during the experiment, as it is highlight by the peak found at 228.4 eV (Fig. 7b). The accompanying peaks of the spectrum correspond to molybdenum oxide peaks, mostly

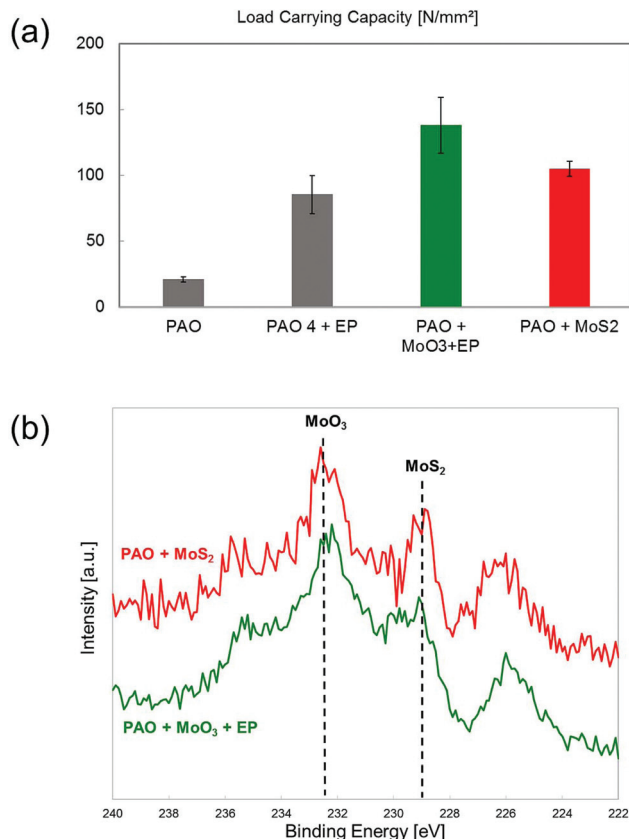


Fig. 7 Investigations using a Brugger test: (a) load carrying capacity according to Brugger for the investigated lubricant mixtures. (b) Mo 3d spectrum measured using XPS on samples lubricated using  $\text{MoO}_3$  nanotubes with the S-containing EP additive. The spectrum measured on samples lubricated with  $\text{MoS}_2$  nanotubes is shown as a reference.

$\text{MoO}_3$  in the presence of  $\text{MoO}_2$  at 231.9 and 230.0 eV, respectively. These peaks can indicate either that not all oxide nanotubes reacted during the experiment or that *in situ* formed  $\text{MoS}_2$  oxidized during the experiment. As a reference, we performed a series of experiments using a lubricant mixture with  $\text{MoS}_2$  nanotubes. The results show that the LCC is slightly lower than the one achieved by the combination of  $\text{MoO}_3$  and the EP additive, but still higher than the reference experiments run using EP the additive. As mentioned, the lubrication mechanism is well-known in this case and relies on the formation of complex tribofilms containing a mixture of Mo and Fe sulfides and oxides.<sup>34</sup> Paradoxically, the spectrum obtained for this lubricant using XPS is extremely similar to the one obtained using  $\text{MoO}_3$  and EP: under severe sliding contact conditions,  $\text{MoS}_2$  nanotubes exfoliate on the surface leaving  $\text{MoS}_2$  platelets attached to the surface and react with the substrate producing  $\text{FeS}$  and  $\text{FeSO}_4$  compounds but also partly degrade leading to the formation of  $\text{MoO}_3$ . On the other hand,  $\text{MoO}_3$  partly sulfurizes in the presence of S containing EP additives, leading to the *in situ* formation of  $\text{MoS}_2$ . According to the results, the latter offers a better lubricity probably due to the continuous formation of  $\text{MoS}_2$  during the sliding process,





as a consequence of the presence of S. The same phenomenon was observed by Aldana *et al.* when using IF-WS<sub>2</sub> nanoparticles at 100 °C in reciprocating sliding.<sup>39</sup> The authors found a higher sulfide to oxide ratio under the presence of ZDDP when compared to the presence of nanoparticles alone, which can be partly justified by the exfoliation of WS<sub>2</sub> platelets on top of the formed ZDDP tribofilm but also due to the *in situ* re-sulfurization of oxidized nanoparticles.

## 4. Conclusions


We showed that MoO<sub>3</sub> nanotubes can be sulfurized *in situ* during sliding contact. The sulfurization results in an excellent friction and wear performance comparable to or even better than that achieved using MoS<sub>2</sub> nanotubes, depending on the severity of the contact conditions. The reason is that under demanding conditions, MoS<sub>2</sub> nanotubes are known to oxidize at the contact interface, while the combination of MoO<sub>3</sub> nanotubes and sulfur compounds leads to a constant sulfurization on-demand. The *in situ* sulfurization process relies on the presence of sulfur containing compounds such as zinc dialkyl dithiophosphate and sulfurized olefin polysulphide. Both compounds are of high technological relevance and currently lack alternatives, thus making them unavoidable in current lubricant formulations. Particularly, the use of ZDDP anti-wear additives in lubricants is ubiquitous and a replacement candidate is not yet in sight. Therefore, by using our approach, MoO<sub>3</sub> nanotubes could fulfil the role of a friction modifier in combination with ZDDP and be able to replace organo molybdenum compounds, which pose serious environmental concerns. In a later stage, the feasibility of using environmentally acceptable sulfur compounds for the *in situ* generation of transition metal dichalcogenides during sliding contact should be explored in order to move towards greener lubrication concepts.

## Conflicts of interest

There are no conflicts of interest to declare.

## Acknowledgements

This work was funded by the Austrian COMET Programme (Project K2 Xtribology. No. 849109) and carried out at the "Excellence Centre of Tribology".

This project has received funding from the European Union's Horizon 2020  research and innovation programme under the Marie Skłodowska-Curie grant agreement No 665778. Co-author A. Tomala acknowledges the POLONEZ project by National Science Centre, Poland under fellowship registration number 2015/19/P/ST8/02597.

## References

- 1 H. P. Jost, *Tribol. Lubr. Technol.*, 2005, **61**, 18–22.
- 2 K. Holmberg, P. Andersson and A. Erdemir, *Tribol. Int.*, 2012, **47**, 221–234.
- 3 W. J. Bartz, *Tribol. Int.*, 2006, **39**, 728–733.
- 4 J. C. Spear, B. W. Ewers and J. D. Batteas, *Nano Today*, 2015, **10**, 301–314.
- 5 E. Gibney, *Nature*, 2015, **522**, 274–276.
- 6 B. J. Irving, P. Nicolini and T. Polcar, *Nanoscale*, 2017, **9**, 5597–5607.
- 7 H. Waghay, T.-S. Lee and B. J. Tatarchuk, *Surf. Coat. Technol.*, 1995, **76–77**, 415–420.
- 8 R. Tenne, L. Margulis, M. Genut and G. Hodes, *Nature*, 1992, **360**, 444–446.
- 9 Y. Feldman, E. Wasserman, D. J. Srolovitz and R. Tenne, *Science*, 1995, **267**, 222–225.
- 10 L. Rapoport, Y. Bilik, Y. Feldman, M. Homyonfer, S. R. Cohen and R. Tenne, *Nature*, 1997, **387**, 791–793.
- 11 M. Remškar, Z. Škraba, M. Regula, C. Ballif, R. Sanjinés and F. Lévy, *Adv. Mater.*, 1998, **10**, 246–249.
- 12 A. Rothschild, R. Tenne, J. Sloan, A. P. E. York, M. L. H. Green, J. Sloan and J. L. Hutchison, *Chem. Commun.*, 1999, 363–364.
- 13 I. Wiesel, R. Popovitz-Biro and R. Tenne, *Nanoscale*, 2013, **5**, 1499.
- 14 J. Tannous, F. Dassenoy, I. Lahouij, T. Le Mogne, B. Vacher, A. Bruhács and W. Tremel, *Tribol. Lett.*, 2011, **41**, 55–64.
- 15 M. Kalin, J. Kogovšek and M. Remškar, *Wear*, 2013, **303**, 480–485.
- 16 V. B. Niste and M. Ratoi, *Mater. Today Commun.*, 2016, **8**, 1–11.
- 17 A. Tomala, B. Vengudusamy, M. Rodríguez Ripoll, A. Naveira Suarez, M. Remškar and R. Rosentsveig, *Tribol. Lett.*, 2015, **59**, 1–18.
- 18 Z. Chen, X. Liu, Y. Liu, S. Gunsell and J. Luo, *Sci. Rep.*, 2015, **5**, 12869.
- 19 C. M. Orofeo, S. Suzuki, Y. Sekine and H. Hibino, *Appl. Phys. Lett.*, 2014, **105**, 83112.
- 20 R. Morrish, T. Haak and C. A. Wolden, *Chem. Mater.*, 2014, **26**, 3986–3992.
- 21 D. Kong, H. Wang, J. J. Cha, M. Pasta, K. J. Koski, J. Yao and Y. Cui, *Nano Lett.*, 2013, **13**, 1341–1347.
- 22 Z. He and W. Que, *Appl. Mater. Today*, 2016, **3**, 23–56.
- 23 M. Remškar, M. Viršek and A. Mrzel, *Appl. Phys. Lett.*, 2009, **95**, 2–4.
- 24 F. Leonard-Deepak, C. F. Castro-Guerrero, S. Mejía-Rosales and M. José-Yacamán, *Nanoscale*, 2011, **3**, 5076.
- 25 M. H. Heyne, D. Chiappe, J. Meererschaut, T. Nuytten, T. Conard, H. Bender, C. Huyghebaert, I. P. Radu, M. Caymax, J.-F. de Marneffe, E. C. Neyts and S. De Gendt, *J. Mater. Chem. C*, 2016, **4**, 1295–1304.
- 26 X. Zhang, B. Luster, A. Church, C. Muratore, A. a Voevodin, P. Kohli, S. Aouadi and S. Talapatra, *ACS Appl. Mater. Interfaces*, 2009, **1**, 735–739.



- 27 N. A. Kumar, M. A. Dar, R. Gul and J.-B. Baek, *Mater. Today*, 2015, **18**, 286–298.
- 28 A. L. Elías, N. Perea-López, A. Castro-Beltrán, A. Berkdemir, R. Lv, S. Feng, A. D. Long, T. Hayashi, Y. A. Kim, M. Endo, H. R. Gutiérrez, N. R. Pradhan, L. Balicas, T. E. Mallouk, F. López-Urías, H. Terrones and M. Terrones, *ACS Nano*, 2013, **7**, 5235–5242.
- 29 J.-K. Huang, J. Pu, C.-L. Hsu, M.-H. Chiu, Z.-Y. Juang, Y.-H. Chang, W.-H. Chang, Y. Iwasa, T. Takenobu and L.-J. Li, *ACS Nano*, 2014, **8**, 923–930.
- 30 S. Li, S. Wang, D.-M. Tang, W. Zhao, H. Xu, L. Chu, Y. Bando, D. Golberg and G. Eda, *Appl. Mater. Today*, 2015, **1**, 60–66.
- 31 M. Kalin, *Mater. Sci. Eng. A*, 2004, **374**, 390–397.
- 32 M. Ratoi, V. B. Niste and J. Zekonyte, *RSC Adv.*, 2014, **4**, 21238.
- 33 A. Varlec, D. Arčon, S. D. Škapin and M. Remškar, *Mater. Chem. Phys.*, 2016, **170**, 154–161.
- 34 A. Tomala, M. Rodríguez Ripoll, C. Gabler, M. Remškar and M. Kalin, *Tribol. Int.*, 2017, **110**, 140–150.
- 35 A. Morina, A. Neville, M. Priest and J. H. Green, *Tribol. Int.*, 2006, **39**, 1545–1557.
- 36 B. C. Windom, W. G. Sawyer and D. W. Hahn, *Tribol. Lett.*, 2011, **42**, 301–310.
- 37 P. U. Aldana, B. Vacher, T. Le Mogne, M. Belin, B. Thiebaud and F. Dassenoy, *Tribol. Lett.*, 2014, **56**, 249–258.
- 38 M. Viršek, A. Jesih, I. Milošević, M. Damnjanović and M. Remškar, *Surf. Sci.*, 2007, **601**, 2868–2872.
- 39 P. U. Aldana, B. Vacher, T. Le Mogne, M. Belin, B. Thiebaud and F. Dassenoy, *Tribol. Lett.*, 2014, **56**, 249–258.
- 40 P. U. Aldana, F. Dassenoy, B. Vacher, T. Le Mogne and B. Thiebaud, *Tribol. Int.*, 2016, **102**, 213–221.
- 41 B. Podgornik, S. Jacobson and S. Hogmark, *Surf. Coat. Technol.*, 2005, **191**, 357–366.
- 42 V. Totolin, M. Rodríguez Ripoll, M. Jech and B. Podgornik, *Tribol. Int.*, 2016, **94**, 269–278.
- 43 M. Ratoi, V. B. Niste, J. Walker and J. Zekonyte, *Tribol. Lett.*, 2013, **52**, 81–91.
- 44 A. Tomala, B. Vengudusamy, M. Rodríguez Ripoll, A. Naveira Suarez, M. Remškar and R. Rosentsveig, *Tribol. Lett.*, 2015, **59**, 26.
- 45 D. N. Khaemba, A. Neville and A. Morina, *Tribol. Lett.*, 2015, **59**, 1–17.
- 46 V. B. Niste and M. Ratoi, *Mater. Today Commun.*, 2016, **8**, 1–11.

